



Yang, T. and Bozhko, S.V. and Asher, G.M. (2015) Active front-end rectifier modelling using dynamic phasors for more-electric aircraft applications. IET Electrical Systems in Transportation, 5 (2). pp. 77-87. ISSN 2042-9738

**Access from the University of Nottingham repository:**

[http://eprints.nottingham.ac.uk/32273/1/Active%20Front-End%20Rectifier%20Modelling%20Using%20Dynamic%20Phasors%20for%20More-Electric%20Aircraft%20Applications\\_IET\\_V5.pdf](http://eprints.nottingham.ac.uk/32273/1/Active%20Front-End%20Rectifier%20Modelling%20Using%20Dynamic%20Phasors%20for%20More-Electric%20Aircraft%20Applications_IET_V5.pdf)

**Copyright and reuse:**

The Nottingham ePrints service makes this work by researchers of the University of Nottingham available open access under the following conditions.

- Copyright and all moral rights to the version of the paper presented here belong to the individual author(s) and/or other copyright owners.
- To the extent reasonable and practicable the material made available in Nottingham ePrints has been checked for eligibility before being made available.
- Copies of full items can be used for personal research or study, educational, or not-for-profit purposes without prior permission or charge provided that the authors, title and full bibliographic details are credited, a hyperlink and/or URL is given for the original metadata page and the content is not changed in any way.
- Quotations or similar reproductions must be sufficiently acknowledged.

Please see our full end user licence at:

[http://eprints.nottingham.ac.uk/end\\_user\\_agreement.pdf](http://eprints.nottingham.ac.uk/end_user_agreement.pdf)

**A note on versions:**

The version presented here may differ from the published version or from the version of record. If you wish to cite this item you are advised to consult the publisher's version. Please see the repository url above for details on accessing the published version and note that access may require a subscription.

For more information, please contact [eprints@nottingham.ac.uk](mailto:eprints@nottingham.ac.uk)

# Active Front-End Rectifier Modelling Using Dynamic Phasors for More-Electric Aircraft Applications

**T. Yang, S. V. Bozhko, G. M. Asher**

The University of Nottingham, Nottingham NG7 2RD, UK

This paper is a postprint of a paper submitted to and accepted for publication in IET Electrical Systems in Transportation and is subject to Institution of Engineering and Technology Copyright. The copy of record is available at IET Digital Library

Corresponding Author: Dr Tao Yang  
Power Electronics, Machine and Control Group  
Institute for Aerospace Technology  
The University of Nottingham  
Nottingham NG7 2RD  
United Kingdom

Phone: +44 (0)115 7484739  
Email: Tao.Yang@nottingham.ac.uk

**Abstract— The More-Electric Aircraft (MEA) has become a dominant trend for next-generation aircraft. The Electrical Power System (EPS) on-board may take many forms: AC, DC, hybrid, frequency-wild, variable voltage, together with the possibility of novel connectivity topologies. To address the stability, availability and capability issues as well as to assess the performance of the power quality and transient behaviour, extensive simulation work is required to develop the EPS architectures. The paper develops a fast-simulation model of active front-end rectifiers based on the dynamic phasor concept. The model is suitable for accelerated simulation studies of EPS under normal, unbalanced and line fault conditions. The performance and effectiveness of the developed model have been demonstrated by comparison against time-domain models in three-phase and synchronous space-vector representations. The experimental verification of the dynamic phasor model is also reported. The prime purpose of the model is for the simulation studies of MEA power architectures at system level; however it can be directly applied for simulation study of any other EPS interfacing with active front-end rectifiers.**

Index Terms – AC-DC power conversion, Aircraft Power Systems, Converters, Dynamics, Modelling, Rectifiers, Vectors.

## I. INTRODUCTION

In recent years there has been significant penetration of power electronics into Electrical Power Systems (EPS). Terrestrial EPS's, particularly at distribution level, promises a multiplicity of Power Electronic Converter (PEC) units handling renewable interfacing, energy storage and EPS conditioning. A similar scenario pertains for the More Electric Aircraft (MEA) and other mobile EPSs. In the MEA for example, the electrification of on-board power will require power electronic conversion to handle power distribution, flight actuation, landing gear, and other functions [1], [2].

The use of large numbers of PECs and their associated control systems has led to significant modelling challenges at the EPS system level due both to system complexity and the wide variation in time constants. For EPS simulations the challenge is to balance the simulation speed against the model accuracy. This is dependent on the modelling task. Power harmonic and Electromagnetic Capacity (EMC) studies, for example, require high bandwidth, switching converter models (of various complexity) and it is appropriate, and often only possible, to simulate a subset of the EPS system. On the other hand, when assessing EPS-system level effects such as system stability, power control and management, load dispatching, fault performance and imbalance, there is little added value in using switching models since the converter switching and harmonics generally have little influence upon the low frequency system dynamics. For MEA simulations, the different modelling bandwidths for different tasks are represented in a four-layer modelling paradigm [3]-[5]. These are: architectural modelling (zero-bandwidth - dc and state events); functional modelling (bandwidth to  $\approx 30\%$  of the AC frequency  $f_c$  with  $< 5\%$  error); behavioural modelling (bandwidths of 100s of kHz and covering converter switching); and component models with no bandwidth limit.

In order to achieve acceptable simulation times for system level EPS modelling, a number of approaches have been exploited. Average state-space models [6], [7] are a standard technique for considering only the fundamental wave behaviour of PECs. For AC distribution systems, it is also desirable to transform the EPS AC signals to the baseband frequency where steady state variables become DC resulting in very fast computation under steady state conditions. Transforming all AC variables to a synchronous rotating frame, henceforth termed the dq0 model, is a known and effective technique [5], [8]. In contrast, a model in which three-phase AC variables are the solution variables is henceforth called an abc model.

One of the disadvantages of the dq0 approach is that under faulted and unbalanced conditions  $2f_c$  components appear and the simulation time steps must be drastically reduced to maintain accuracy; under such conditions the dq0 approach simulates slower than the abc model. An alternative approach that can address this problem is that of Dynamic Phasors (DPs) [9], [10]. The  $k^{\text{th}}$  order DP is the complex time-varying coefficients of the  $k^{\text{th}}$  Fourier harmonic derived over a moving time windowed signal. The modelling accuracy and bandwidth is selected by choosing the window length and the

harmonic order. Considering only the significant harmonic components, the DP model is capable of retaining the dominant dynamic features of an EPS and is ideally suited for functional non-switching EPS modelling. Again, under steady-state conditions, the DP variable is a complex dc quantity and simulation is rapid. Under steady state imbalanced conditions, the 3 complex DP variables (one per phase) are still dc valued resulting in much better computational performance compared with the dq0 approach.

The DP method has been applied to the modelling of terrestrial EPS including unbalanced regimes [10]-[12]. A comparative study of a simple EPS with line faults, carried out in the abc, dq0 and DP domains, is given in [13] where the efficiency of the DP approach is demonstrated. The DP method has also been applied to synchronous and induction machines [14], [15] and Doubly-Fed Induction Generators (DFIG) [16]. Flexible AC Transmission System (FACTS) devices [17], [18], including active filters [19] and STATCOMs [20], [21] have also been reported. In [22], [23], a DP model for thyristor-based HVDC transmission systems is reported, although only balanced conditions are considered. In [24] the DP model of Voltage-Source Converter based (VSC) HVDC is reported; here authors approximate the converter's Pulse-Width Modulation (PWM) by the fundamental wave component of switching function that was derived assuming symmetrical balanced operation.

In order to handle EPS with PECs in both balanced and unbalanced AC conditions, a general DP representation of three-phase AC-DC converters is required. The two most typical representatives of this converter class are the uncontrolled diode rectifier (in MEA applications it is often used in conjunction with an autotransformer [2]) and the PWM active front-end rectifier using IGBTs. This paper addresses this general representation first through the consideration of the controlled PWM rectifier. Henceforth this will be termed the Controlled Rectifier Unit or CRU. A follow on paper will cover the case of the diode family which is a more difficult case on account of the existence of discontinuous states and variable switching patterns under AC faulted conditions.

State-average models of the CRU in a synchronous frame were developed in [29], [30] and report good accuracy. Based on these, a non-switching functional dq0 model of CRU was developed in [31] and shown to deliver accuracy within the MEA functional-level requirements. The simulation speed was reported to be three orders of magnitude higher than the abc model incorporating converter switching. However, under unbalanced and line fault operation, the simulation speed reduced significantly and lends motivation for the development of DP models of this paper.

DP modelling of systems containing PWM-controlled CRUs has been reported recently. In [18], a CRU-type converter is considered as a part of the unified power flow controller (UPFC) controlling the power flow between a Synchronous Generator (SG) and the Infinite Bus (IB). Here, the authors derived a DP model base on the dq-frame averaging

model with the d axis orientated on the synchronous rotor frame. The DP model derived in [18] can only be used for modelling elements such as Double-Fed Induction Generator (DFIG) and Unified Power Flow Controller (UPFC). In these cases the DP model is derived from dq-frame averaging model and the d axis is naturally fixed on the machine rotor. However, for the CRU, the d axis is aligned with the voltage vector at the coupling point and the voltage vector angle is not known but derived from a Phase-Locked Loop (PLL). To get round this restriction the authors had to control the CRU using frame-invariant real and reactive power. However, this is in contrast to the typical CRU structures which use active and reactive components of the input current for control; this requires orientation on the voltage vector at the point of connection. In addition only simulation results for a low degree of unbalance are given in [18] and fault capability was not demonstrated. In [20] and [24] a CRU-type converter is also considered as a part of a STATCOM and VSC-HVDC system respectively. However the reported models are applicable for balanced conditions only.

Summarizing all the above, system-level simulation studies of MEA EPS require accurate but time-efficient functional-level models for AC/DC converters capable of reproducing system dynamic behaviour under both normal and abnormal operations. This paper aims to develop a CRU model that exhibits the same computational effectiveness found in dq0 models at balanced conditions but, unlike dq0 models, maintains its effectiveness under both unbalanced and line fault scenarios. In order to reach this goal, this study will exploit some remarkable properties of DPs. The contribution of this paper is as follows:

- The reported model is applicable for significantly accelerated simulations of complex EPS's, both balanced and unbalanced, containing multiple active PWM rectifier feeds; this cannot be represented using the DP based models published so far.
- As an outcome to the above, the PWM active rectifier feeds can be current controlled through orientation at the local point of connection; this cannot be represented using the DP based models published so far.
- The model is verified experimentally and the computational performance is compared against both the corresponding time-domain abc switching model and the functional non-switching dq0 model. A significant computational acceleration for the DP-based model in simulation of different operational scenarios is demonstrated.

## II. DYNAMIC PHASORS

In this section, in order assist readability, the basic DP theory is reviewed [9], [12], [14]. This will be intensively used throughout the rest of the paper.

The DP concept is based on the generalized averaging theory [9] and assumes a time-domain nearly-periodic waveform  $x(\tau)$  can be represented on the interval  $\tau \in (t-T, t]$  by the following Fourier series:

$$x(t) = \sum_{k=-\infty}^{\infty} X_k(t) e^{jk\omega_s t} \quad (1)$$

where  $\omega_s = 2\pi/T$  and  $T$  are the fundamental period of the waveform.  $X_k(t)$  is the  $k^{\text{th}}$  Fourier coefficient in complex form referred to as a “dynamic phasor” (DP) and determined as follows:

$$X_k(t) = \frac{1}{T} \int_{t-T}^t x(\tau) e^{-jk\omega_s \tau} d\tau = \langle x \rangle_k(t) \quad (2)$$

where  $k$  is the DP index. In contrast to the traditional Fourier Transformation (FT), these Fourier coefficients are time-varying as the integration interval (window) slides through time. The selected set of DPs, or  $K = \{1, 2, \dots, k, \dots\}$ , defines the approximation accuracy of the waveform. For example, for dc-like variables and signals the index set only includes the component  $K = \{0\}$ , and for purely sinusoidal ones  $K = \{1\}$ . It is crucial to notice that an interface between time-domain models and DP models can be developed based on (2).

A key factor in developing dynamic models based on DPs is the relation between the derivatives of the variable  $x(t)$  and the derivatives of  $k^{\text{th}}$  Fourier coefficients given as [9], [10]:

$$\left\langle \frac{dx}{dt} \right\rangle_k(t) = \frac{dX_k(t)}{dt} + jk\omega_s X_k(t) \quad (3)$$

This can be verified using (1), (2), and be used in evaluating the  $k^{\text{th}}$  phasor of time-domain model. The differential term on the right side of (3) is crucial. This term allows the DP to study transient behaviour of signals. If we drop this term, the differential property of DP reduces to be the same as that of traditional phasors.

Another important property of DP is that the  $k^{\text{th}}$  phasor of a product of two time-domain variables can be obtained via the convolution of corresponding DPs:

$$\langle xy \rangle_k = \sum_i \langle x \rangle_{k-i} \langle y \rangle_i \quad (4)$$

The properties of (3) and (4) play a key role when transforming the time-domain models into the DP domain. Algebraic manipulations in this paper will also exploit the following property of real functions  $x(\tau)$ :

$$X_{-k}(t) = X_k^*(t) \quad (5)$$

where the notation  $*$  denotes a complex conjugate.

### III. CRU MODELLING USING DYNAMIC PHASORS

The active front-end CRU is well-known from previous publications [25], [30] and in its basic form is shown in Fig.1. A key requirement for the model being developed is the capability of time-efficient simulation of CRU operation under both balanced and unbalanced operational conditions, with the required accuracy according to the functional modelling level specification (within 5% envelope of the behavioural-level model waveform [4], [5]).

This converter allows for independent control of active and reactive power flow via the control of the AC current components expressed in a synchronously rotating frame. The direct axis is aligned with the voltage vector at the point of connection. In terms of three-phase quantities, this voltage can be expressed as follows:

$$\bar{v} = \frac{2}{3} (v_a + v_b e^{j2\pi/3} + v_c e^{j4\pi/3}) \quad (6)$$

where  $v_a$ ,  $v_b$  and  $v_c$  are phase voltages at the point of connection. The voltage vector angular position  $\theta$  is normally derived by a PLL. The PLL itself is a control system with its own dynamics. Modern PLL structures [32] perform a very accurate voltage tracking. Therefore, for the purpose of this study, we can assume that the PLL in Fig.1 delivers the exact value of  $\theta$  for any set of phase voltages  $v_a$ ,  $v_b$ ,  $v_c$ , including cases of severe voltage unbalance and phase displacement.

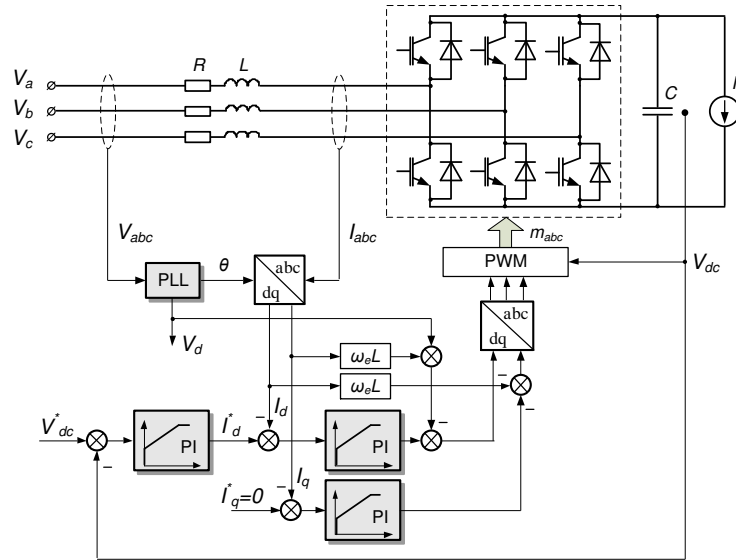


Fig. 1 Active front-end rectifier control structure

Basically, the reported model is derived by transforming the time-domain CRU dynamic equations into the frequency-domain DP form. The model development process can be conditionally broken-down into the following key stages:

- Establishing how to map the generally unbalanced time-domain CRU supply voltage vector (6) into DPs. Since CRU operation and control require decomposition of the voltage vector (6) into synchronously rotating frame components, it is essential to establish how the DPs of these components can be derived from time-domain values of individual phase voltages  $v_a$ ,  $v_b$  and  $v_c$ . Furthermore, it is necessary to establish how these components will behave during balanced and unbalanced conditions;
- Since the CRU control is based on controlled current components oriented on a rotating frame aligned to a voltage vector (6), these components are mapped into the DP domain for subsequent use in CRU control;
- Transforming the CRU control structure into DPs;
- Transforming the power conversion stage into the DP domain. The functional modelling level requirement means that a non-switching model of the power conversion is used.

In the text below, the model development process is reported according these stages.

#### A. Voltage and Current Vector

In this section we establish how, using three-phase time-domain values of abc voltages, one can derive the DPs for the synchronously rotating frame components of generally unbalanced CRU input voltages.

Assuming the CRU is supplied by the three-phase voltage with the following individual phase components:

$$v_i = V_i \cos(\omega t + \varphi_i), \quad i=a,b,c \quad (7)$$

where  $V_i$  is the phase voltage magnitude and  $\varphi_i$  is the corresponding phase angle. The DPs of (7) can be derived according to the DP definition (2). Selecting the DP set as  $K=\{1\}$  since (7) includes only the fundamental component, we have:

$$\langle v_i \rangle_1 = \frac{1}{T} \int_{t-T}^t V_i \cos(\omega \tau + \varphi_i) e^{-j\omega \tau} d\tau = \frac{1}{2} V_i e^{j\varphi_i}, \quad i = a,b,c \quad (8)$$

As one can see from (8), these DPs are just complex numbers. It is important to notice that the DP  $\langle v_i \rangle_1$  is half of its corresponding traditional phasors  $\dot{V}_i$ . Substituting (7) and (8) into (6) and re-arranging the terms results in the following relation:

$$\vec{v} = \frac{2}{3} e^{j\omega t} \left[ \langle v_a \rangle_1 + \langle v_b \rangle_1 e^{j2\pi/3} + \langle v_c \rangle_1 e^{-j2\pi/3} \right] + \frac{2}{3} e^{-j\omega t} \left[ \langle v_a \rangle_1^* + \langle v_b \rangle_1^* e^{j2\pi/3} + \langle v_c \rangle_1^* e^{-j2\pi/3} \right] \quad (9)$$

This equation shows how the voltage vector (6) can be defined through DP components. It is clearly seen that the two right-hand side terms define the positive and the negative sequences of the input voltage vector respectively. The latter will only

appear when phase voltages are unbalanced. Using (9), the DPs for voltage vector components in a synchronously rotating reference frame can now be derived.

Considering the stationary  $\alpha\beta$  reference frame in which the voltage vector can be expressed as:

$$\vec{v} = \vec{v}_{\alpha\beta} = |\mathbf{v}|e^{j\alpha+\varphi} = v_{\alpha} + jv_{\beta} \quad (10)$$

where  $\vec{v}_{\alpha\beta}$  represents voltage vector in the  $\alpha\beta$  frame. The components  $v_{\alpha}$  and  $v_{\beta}$  are the real and the imaginary parts of (9). Under balanced conditions,  $|\mathbf{v}|$  and  $\varphi$  are constant and equal to  $V_a$  and  $\varphi_a$  respectively. In general cases, the magnitude  $|\mathbf{v}|$  and the angle  $\varphi$  are not necessarily constant and depend on the magnitudes and phase angles of all individual phase voltages in (7). In general, both these values are time-dependent, i.e.  $|\mathbf{v}|=|\mathbf{v}|(t)$  and  $\varphi=\varphi(t)$ .

A reference frame dq is now introduced. This frame rotates synchronously with the speed corresponding to the base EPS frequency  $\omega=2\pi f_e$ , as shown in Fig.2. The input voltage vector in terms of the dq frame can be derived from  $\alpha\beta$ -frame representation in a simple manner:

$$\vec{v}_{dq} = \vec{v}_{\alpha\beta}e^{-j\alpha} = v_d + jv_q \quad (11)$$

Substituting (9) and (10) into (11) results in:

$$\vec{v}_{dq} = (V_{d0} + jV_{q0}) + (V_{d2} + jV_{q2})e^{-j2\alpha} \quad (12)$$

where variables  $V_{d0}$ ,  $V_{q0}$ ,  $V_{d2}$  and  $V_{q2}$  can be calculated as:

$$V_{d0} = \frac{2}{3} \text{Re}[\langle v_a \rangle_1 + \langle v_b \rangle_1 e^{j2\pi/3} + \langle v_c \rangle_1 e^{-j2\pi/3}] \quad (13a)$$

$$V_{q0} = \frac{2}{3} \text{Im}[\langle v_a \rangle_1 + \langle v_b \rangle_1 e^{j2\pi/3} + \langle v_c \rangle_1 e^{-j2\pi/3}] \quad (13b)$$

$$V_{d2} = \frac{2}{3} \text{Re}[\langle v_a \rangle_1^* + \langle v_b \rangle_1^* e^{j2\pi/3} + \langle v_c \rangle_1^* e^{-j2\pi/3}] \quad (13c)$$

$$V_{q2} = \frac{2}{3} \text{Im}[\langle v_a \rangle_1^* + \langle v_b \rangle_1^* e^{j2\pi/3} + \langle v_c \rangle_1^* e^{-j2\pi/3}] \quad (13d)$$

The equations (12), (13) define a general voltage vector in a synchronous dq frame expressed with the DPs of individual phase voltages  $\langle v_i \rangle_1$ . Analysis of (12) shows that the variables  $V_{d0}$  and  $V_{q0}$  define the positive sequence of the voltage whilst  $V_{d2}$  and  $V_{q2}$  define the negative one.

The d- and q- axis components of the input voltage vector  $v_d$  and  $v_q$  can be derived from (12) by separation of real and imaginary parts:

$$v_d = \text{Re}(\vec{v}_{dq}) = V_{d0} + V_{d2} \cos 2\alpha + V_{q2} \sin 2\alpha \quad (14)$$

$$v_q = \text{Im}(\tilde{v}_{dq}) = V_{q0} + V_{q2} \cos 2\omega t - V_{d2} \sin 2\omega t \quad (15)$$

The following can be concluded from (14) and (15):

- Under balanced conditions the voltage dq-components become DC-like:  $v_d = V_{d0}$  and  $v_q = V_{q0}$ .
- If the supply voltage is unbalanced, the dq frame components of the voltage vector will include components of the doubled frequency as well as the dc components  $V_{d0}$  and  $V_{q0}$ .
- The DP set  $K$ , representing a general supply voltage in synchronously rotating dq frame should include DC and 2<sup>nd</sup> harmonics, i.e.

$$K = \{0, 2\} \quad (16)$$

The DPs for the CRU input voltage vector dq-frame components are given in Table I together with the DPs for the input current  $\vec{i}$  derived in a similar manner.

TABLE I. DPs FOR CRU INPUT VOLTAGE AND CURRENT IN SYNCHRONOUSLY ROTATING FRAME

Variable	DPs	
	k=0	k=2
$v_d$	$\langle v_d \rangle_0 = V_{d0}$	$\langle v_d \rangle_2 = (V_{d2} - jV_{q2})/2$
$v_q$	$\langle v_q \rangle_0 = V_{q0}$	$\langle v_q \rangle_2 = (V_{q2} + jV_{d2})/2$
$i_d$	$\langle i_d \rangle_0 = I_{d0}$	$\langle i_d \rangle_2 = (I_{d2} - jI_{q2})/2$
$i_q$	$\langle i_q \rangle_0 = I_{q0}$	$\langle i_q \rangle_2 = (I_{q2} + jI_{d2})/2$

Hence, the mapping of the synchronously rotating reference frame components of the CRU input voltage and current into the frequency domain of DPs is established.

### B. Active and Reactive Current Components

Operation of the CRU requires an independent control of the input current components with respect to the input voltage vector as shown in Fig.2. We define a new rotating frame, DQ frame, and align the D-axis with the voltage vector, under both balanced and unbalanced conditions. Under balanced conditions, this DQ frame will move synchronously with the frame dq defined in the previous section. During unbalance, the voltage vector (9), and hence the DQ frame as well, will exhibit a complex motion with double-frequency components with respect to the dq frame according to (13). Hence, the DPs for the input currents in the DQ-frame components (denoted as  $i_D$  and  $i_Q$ ) are required. This is the subject of this section.

The relation between the input current components in the DQ and dq frames at any instant can be derived from the geometry in Fig.2:

$$i_D = i_d \cos \phi + i_q \sin \phi \quad (17)$$

$$i_Q = -i_d \sin \phi + i_q \cos \phi \quad (18)$$

where  $\phi$  is the angle between d axis and D axis.

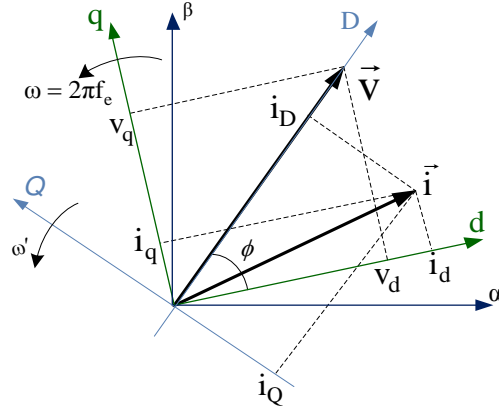


Fig. 2. Frame considerations for developing DP CRU model

Mapping (17) and (18) into the DP involves the application of the convolution property in (4). In addition to knowledge of the DPs for  $i_d$  and  $i_q$  (derived in the previous section), one needs to establish the DPs for  $\sin \phi$  and  $\cos \phi$  due to the time-varying  $\phi$ . From the geometry of Fig.2, they can be expressed via d and q axes voltage components:

$$\cos \phi = f_1(v_d, v_q) = v_d / \sqrt{v_d^2 + v_q^2} \quad (19)$$

$$\sin \phi = f_2(v_d, v_q) = v_q / \sqrt{v_d^2 + v_q^2} \quad (20)$$

The transformation of non-linear functions (19), (20) into the DP domain (i.e. calculation of the DPs  $\langle \sin \phi \rangle_k$  and  $\langle \cos \phi \rangle_k$  by directly applying (2), (12) and (13)) is not analytical. We therefore propose expanding (19) and (20) into a Taylor series with respect to  $v_d$  and  $v_q$  followed by the transformation of the truncated series into the DP domain. This is now described.

Approximating (19) and (20) by the Taylor series requires selection of the operational point for the expansion. The natural choice is the voltage dq components corresponding to the positive sequence of the voltage vector. Hence, the operating point is defined as  $\{V_{d0}, V_{q0}\}$  according to (12). The Taylor expansion of (19) and (20) yields:

$$\cos \phi \approx k_{10} + \frac{k_{11}}{1!}(v_d - V_{d0}) + \frac{k_{12}}{1!}(v_q - V_{q0}) + \frac{k_{13}}{2!}(v_d - V_{d0})^2 + \frac{k_{14}}{2!}(v_q - V_{q0})^2 + \frac{k_{15}}{2!}(v_d - V_{d0})(v_q - V_{q0}) + \dots \quad (21)$$

$$\sin \phi \approx k_{20} + \frac{k_{21}}{1!}(v_d - V_{d0}) + \frac{k_{22}}{1!}(v_q - V_{q0}) + \frac{k_{23}}{2!}(v_d - V_{d0})^2 + \frac{k_{24}}{2!}(v_q - V_{q0})^2 + \frac{k_{25}}{2!}(v_d - V_{d0})(v_q - V_{q0}) + \dots \quad (22)$$

where  $k_j$  are constant coefficients depending on the selected operation point. These can be calculated using (13), (19)-(20)

and are given in Appendix I.

The series (21) and (22) can be converted into the frequency domain after suitable truncation. Traditionally only the first-order terms are considered. Due to the DP convolution property (4), converting high-order terms into DPs is possible and this will improve accuracy. In this study we found that truncating 3<sup>rd</sup>-order and higher terms in (21), (22) provides very good approximations even for very unbalanced fault conditions when  $v_d$  and  $v_q$  in (19) and (20) are severely disturbed by the doubly-frequency components. This will be shown by comparative simulations in following Sections. Applying DP definition (2), convolution property (4) to (21), (22) and using Table I, after some algebraic manipulation, we can derive the following DPs (the set is  $K=\{0,2\}$  as above):

$$\langle \cos \phi \rangle_0 = k_{10} + k_{13} \langle v_d \rangle_2 \langle v_d \rangle_2^* + k_{14} \langle v_q \rangle_2 \langle v_q \rangle_2^* + k_{15} \left( \langle v_d \rangle_2 \langle v_q \rangle_2^* + \langle v_d \rangle_2^* \langle v_q \rangle_2 \right) \quad (23a)$$

$$\langle \cos \phi \rangle_2 = k_{11} \langle v_d \rangle_2 + k_{12} \langle v_q \rangle_2 \quad (23b)$$

$$\langle \sin \phi \rangle_0 = k_{20} + k_{23} \langle v_d \rangle_2 \langle v_d \rangle_2^* + k_{24} \langle v_q \rangle_2 \langle v_q \rangle_2^* + k_{25} \left( \langle v_d \rangle_2 \langle v_q \rangle_2^* + \langle v_d \rangle_2^* \langle v_q \rangle_2 \right) \quad (24a)$$

$$\langle \sin \phi \rangle_2 = k_{21} \langle v_d \rangle_2 + k_{22} \langle v_q \rangle_2 \quad (24b)$$

All the voltage DPs participating in (23), (24) are already derived and given in the Table I. Thus, the frequency-domain images of functions (19), (20) are derived as the DPs (23)-(24). Equations (17) and (18) can now be mapped into the DPs as well using the convolution property (4):

$$\langle i_D \rangle_0 = \langle i_d \rangle_0 \langle \cos \phi \rangle_0 + \langle i_d \rangle_2^* \langle \cos \phi \rangle_2 + \langle i_d \rangle_2 \langle \cos \phi \rangle_2^* + \langle i_q \rangle_0 \langle \sin \phi \rangle_0 + \langle i_q \rangle_2^* \langle \sin \phi \rangle_2 + \langle i_q \rangle_2 \langle \sin \phi \rangle_2^* \quad (25)$$

$$\langle i_Q \rangle_0 = -\langle i_d \rangle_0 \langle \sin \phi \rangle_0 - \langle i_d \rangle_2^* \langle \sin \phi \rangle_2 - \langle i_d \rangle_2 \langle \sin \phi \rangle_2^* + \langle i_q \rangle_0 \langle \cos \phi \rangle_0 + \langle i_q \rangle_2^* \langle \cos \phi \rangle_2 + \langle i_q \rangle_2 \langle \cos \phi \rangle_2^* \quad (26)$$

$$\langle i_D \rangle_2 = \langle i_d \rangle_0 \langle \cos \phi \rangle_2 + \langle i_d \rangle_2 \langle \cos \phi \rangle_0 + \langle i_q \rangle_0 \langle \sin \phi \rangle_2 + \langle i_q \rangle_2 \langle \sin \phi \rangle_0 \quad (27)$$

$$\langle i_Q \rangle_2 = -\langle i_d \rangle_0 \langle \sin \phi \rangle_2 - \langle i_d \rangle_2 \langle \sin \phi \rangle_0 + \langle i_q \rangle_0 \langle \cos \phi \rangle_2 + \langle i_q \rangle_2 \langle \cos \phi \rangle_0 \quad (28)$$

Hence, all DPs constituting the controlled variables – namely  $i_D$  and  $i_Q$ , are derived. From the basic principle of CRU control, the components  $\langle i_D \rangle_2$  and  $\langle i_Q \rangle_2$  should be controlled to zero. The component  $\langle i_Q \rangle_0$  controls the reactive power. The component  $\langle i_D \rangle_0$  controls the active power flow and hence the DC-link voltage.

### C. Dynamic Phasors for the PI controller

As shown in Fig.1, the control structure of the CRU employs Proportional-Integral (PI) controllers that should be

converted into the DP domain as well. The state-space equation for the PI controller in the time domain is:

$$\dot{x} = k_i u, \quad y = k_p u + x \quad (29)$$

where  $u$  is the input, and  $k_p$  and  $k_i$  are the proportional and integral gains correspondingly. This equation can be converted into DPs as:

$$\frac{d\langle x \rangle_k}{dt} = k_i \langle u \rangle_k - jk\omega \langle x \rangle_k; \quad \langle y \rangle_k = k_p \langle u \rangle_k + \langle x \rangle_k \quad (30)$$

The selection of DPs index  $K$  is as (14) with  $K=\{0,2\}$ . Other linear controllers can be handled in a similar fashion.

#### D. Modulation index and transformation to three-phase coordinates

The CRU control output is a three-phase modulation index  $m_{abc}$  (in the three-phase domain) that is derived from the DQ frame index  $m_{DQ}$  produced by the current controllers. The relation between  $m_{DQ}$  and  $m_{abc}$  is:

$$[m_a \ m_b \ m_c]^T = K_s [m_D \ m_Q]^T \quad (31)$$

where the transformation matrix  $K_s$  is given by

$$K_s = \begin{bmatrix} \cos(\omega t + \phi) & -\sin(\omega t + \phi) \\ \cos(\omega t + \phi - 2\pi/3) & -\sin(\omega t + \phi - 2\pi/3) \\ \cos(\omega t + \phi + 2\pi/3) & -\sin(\omega t + \phi + 2\pi/3) \end{bmatrix} \quad (32)$$

As discussed previously, in unbalanced conditions the angle  $\phi$  is not constant, hence  $K_s$  is not constant either. Hence, mapping the coordinate transformation (32) into the DP domain requires knowledge of corresponding DP for matrix  $K_s$ . This can be found in the following way. Each element of  $K_s$  can be re-written as separate  $\phi$ -dependent terms using basic trigonometric rules, for example:

$$\cos(\omega t + \phi - 2\pi/3) = 0.5\{(-\cos \phi + \sqrt{3} \sin \phi) \cos \omega t + (\sin \phi + \sqrt{3} \cos \phi) \sin \omega t\} \quad (33)$$

The corresponding DP can be then derived using the convolution property (4) as detailed below. The terms  $\cos \omega t$  and  $\sin \omega t$  are converted into the DP domain directly applying (2). For these purely harmonic terms the DP index set includes only  $k=1$  as  $\omega$  is constant. The corresponding DPs are:

$$\langle \cos \omega t \rangle_1 = \langle \cos \omega t \rangle_{-1} = \langle \cos \omega t \rangle_1^* = 0.5 \quad (34)$$

$$\langle \sin \omega t \rangle_1 = -0.5j; \quad \langle \sin \omega t \rangle_{-1} = \langle \sin \omega t \rangle_1^* = 0.5j \quad (35)$$

The DPs for  $\cos\phi$  and  $\sin\phi$  are derived in (23) and (24) and the DP set for these is  $\{0, 2\}$  according to (16). Hence, following (4), the DP index set for each element of matrix  $K_s$  should include the 1<sup>st</sup> (fundamental) and the 3<sup>rd</sup> harmonic. Applying (4) to (30), one obtains:

$$\begin{aligned} \langle \cos(\omega t + \phi - 2\pi/3) \rangle_1 &= 0.5 \cdot \langle \cos \omega t \rangle_1 \langle (-\cos \phi + \sqrt{3} \sin \phi) \rangle_0 - 0.5 \cdot \langle \sin \omega t \rangle_1 \langle (\sin \phi + \sqrt{3} \cos \phi) \rangle_0 \\ &\quad + 0.5 \cdot \langle \cos \omega t \rangle_1^* \langle (-\cos \phi + \sqrt{3} \sin \phi) \rangle_2 - 0.5 \cdot \langle \sin \omega t \rangle_1^* \langle (\sin \phi + \sqrt{3} \cos \phi) \rangle_2 \end{aligned} \quad (36)$$

$$\langle \cos(\omega t + \phi - 2\pi/3) \rangle_3 = 0.5 \cdot \langle \cos \omega t \rangle_1 \langle (-\cos \phi + \sqrt{3} \sin \phi) \rangle - 0.5 \cdot \langle \sin \omega t \rangle_1 \langle (\sin \phi + \sqrt{3} \cos \phi) \rangle_2 \quad (37)$$

The DPs for other elements of  $K_s$  can be calculated in a similar way. Applying DP properties (4) and (5), the DP for coordinate transformation (31) can then be established:

$$\left\langle \begin{bmatrix} m_a \\ m_b \\ m_c \end{bmatrix} \right\rangle_1 = \langle K_s \rangle_1 \left\langle \begin{bmatrix} m_D \\ m_Q \end{bmatrix} \right\rangle_0 + \langle K_s \rangle_1^* \left\langle \begin{bmatrix} m_D \\ m_Q \end{bmatrix} \right\rangle_2 + \langle K_s \rangle_3 \left\langle \begin{bmatrix} m_D \\ m_Q \end{bmatrix} \right\rangle_2^* \quad (38)$$

Here  $\langle K_s \rangle_1$  and  $\langle K_s \rangle_3$  are matrixes of the same structure as (32) but constituted by DPs of  $k=1$  and  $k=3$  correspondingly.

#### E. Power conversion

Functional modelling does not require switching converter behaviour. Therefore the power conversion is governed by the following time-domain equations [31]:

$$v_\eta = 0.5 \cdot v_{dc} m_\eta \quad (39)$$

$$i_{dc} = 0.5 \sum_\eta m_\eta i_\eta \quad (40)$$

where  $v_{dc}$  is the dc-link voltage,  $m_\eta$  is the modulation index of the corresponding phase ( $\eta=a,b,c$ ),  $i_\eta$  is the phase current.

Transforming these equations into DPs yields:

$$\langle v_\eta \rangle_k = 0.5 \langle v_{dc} \rangle_0 \langle m_\eta \rangle_k \quad (41)$$

$$\langle i_{dc} \rangle_0 = 0.5 \sum_\eta \langle m_\eta \rangle_k \langle i_\eta \rangle_k^* \quad (42)$$

Here, only the fundamental component is considered on the ac side, so the DP index is chosen as  $k=1$ . For the dc-side variables the set is  $k=0$  since only the dc component is considered.

## F. Assembling the model

The above derived DPs equations constitute the core model of the CRU. As a signal flow diagram the model is given in Fig.3. This model can be directly applied for simulation studies when an entire EPS is modelled in the DP domain, similar to the study reported in [26]. In this case all the required inputs (supply voltages, input currents, DC voltage) are available in the form of DPs, and the outputs of the model (CRU terminal voltages and DC current) can be directly interfaced with the other EPS unit models. The model's signal flow can be easily conceived through comparison of Fig.1 and Fig.3. One notes that in DP domain the DC voltage control remains the same whilst the input current is controlled via its four components derived in (25)-(28). It is natural that all the 2<sup>nd</sup>-order DPs should be controlled to zero, together with main Q-axis current's DP to achieve the unity power factor. It is also seen from Fig.3 that the model order is increased compared to the three-phase domain model; however the AC DP signals are DC-like in steady state and a significant acceleration in simulation is expected (to be confirmed in the following Sections).

The model can be applied to simulation studies of EPS dynamic in a traditional three-phase domain as well. In this case, the model in Fig.3 should be supplemented by the interfacing module as shown in Fig.4 in order to establish a communication between the three-phase and the DP domains. The interfacing module Fig.4 includes the DP calculators based on (2). The interfacing module also includes the DP-domain equations for the input RL circuit to link the CRU terminal voltages and the input currents:

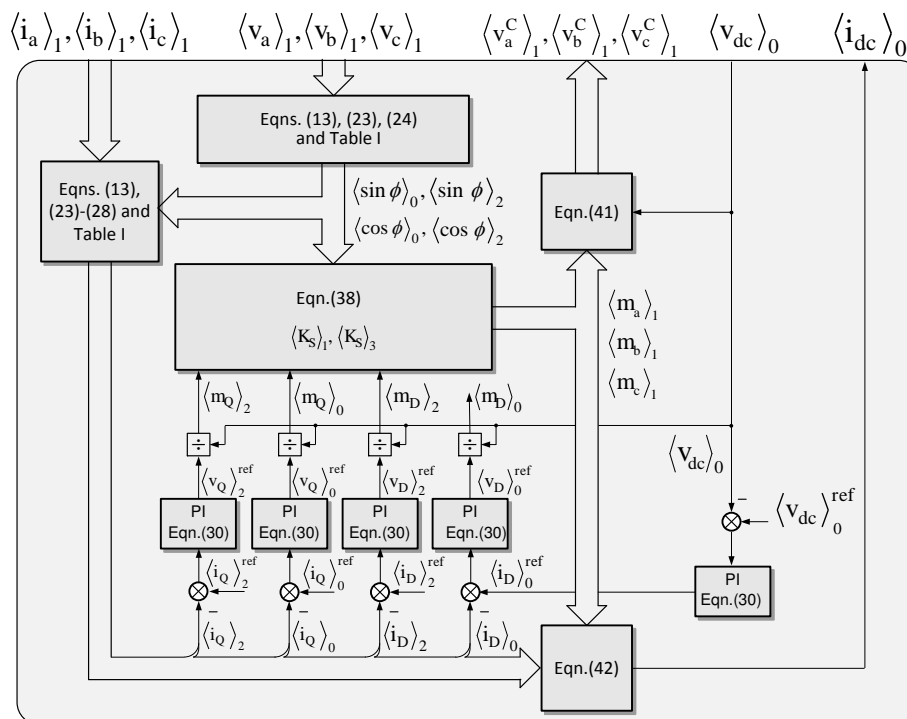


Fig.3. DP domain model of active front-end rectifier

$$L \frac{d\langle i_i \rangle_1}{dt} = -R\langle i_i \rangle_1 - j\omega L\langle i_i \rangle_1 + \langle v_i \rangle_1 - \langle v_i^c \rangle_1, \quad i = a, b, c \quad (43)$$

If the model is implemented according to Fig.4, the end user will be able to build three-phase EPS models, without the necessity of understanding DPs theory.

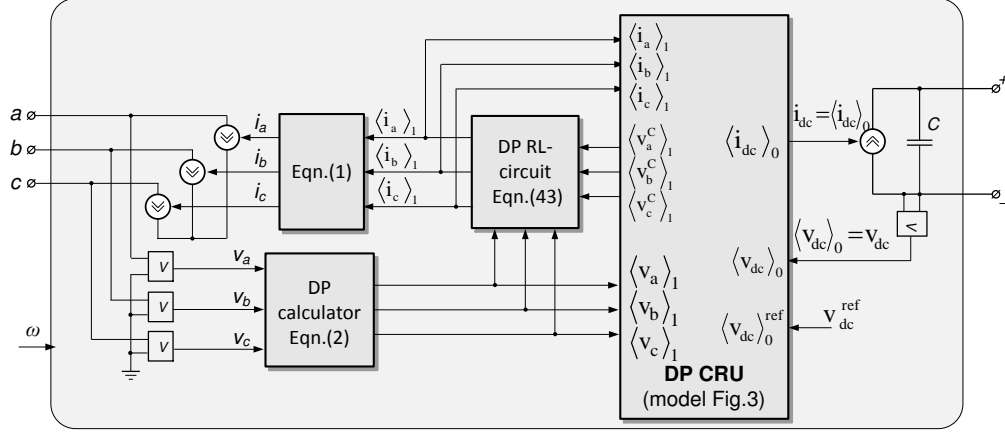


Fig.4. Three-phase interfacing of the DP CRU model

#### IV. MODEL EXPERIMENTAL VERIFICATION

The experiments to verify the model were conducted on a CRU developed for operation as an active shunt filter in an aircraft EPS. The CRU was supplied by a programmable AC source Chroma 61705 capable of generating balanced and unbalanced sets of three-phase voltages. The CRU control is implemented using a Digital Signal Processor TMS320C671 connected to an FPGA board for data acquisition and sampling. The rig parameters are given in Table II below.

TABLE II. EXPERIMENTAL SYSTEM PARAMETERS

Three-phase supply	V=120Vrms, fs=400Hz
Input impedance	L = 3 mH, R = 0.1 $\Omega$
DC-Link capacitor	C = 2200 $\mu$ F
Switching frequency	f <sub>sw</sub> = 10 kHz
Sampling frequency	f <sub>c</sub> = 10 kHz

For aircraft system-level EPS studies, the dynamics of the CRU DC output voltage and the AC input current are of prime importance, therefore these parameters were monitored during the experiments and reported below.

##### A. Balanced operation

In this experiment the CRU was supplied by balanced set of voltages 80Vrms at 400Hz. The CRU was loaded by 200 $\Omega$  resistor ( $\approx$ 15% of the rated power). The DC-link voltage demand was changed from 200V to 270V at t = 2s. The experimental and DP simulated DC-link voltage and CRU input currents responses are shown in Fig.5. As one can conclude,

the model reproduces the transient behaviour of both DC-link voltage and input currents (its main harmonic) with accuracy well within functional-level requirements.

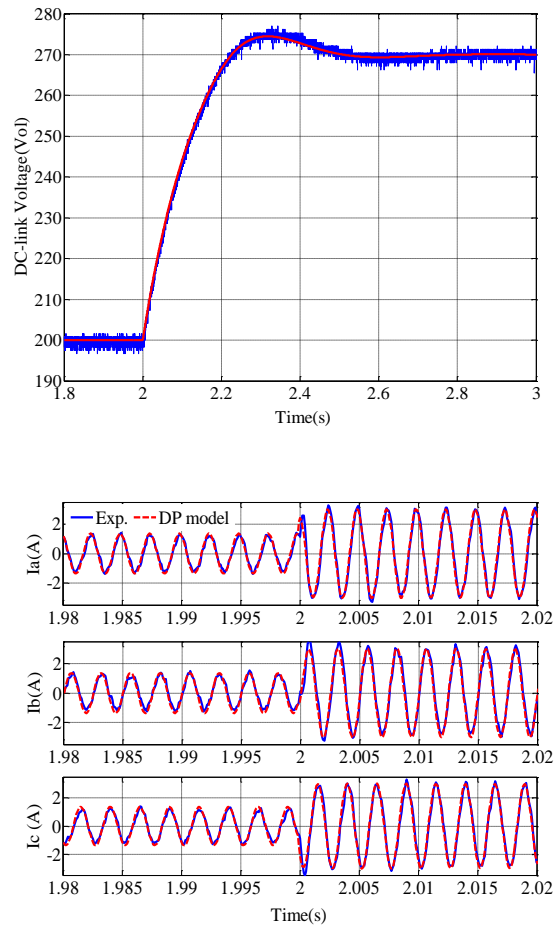


Fig.5. DC voltage (above) and input current (below) in response to a step in voltage demand (blue-experiment, red – model) under the balanced supply

### B. Unbalanced operation

Similar transient conditions were applied in the case of an unbalanced supply. A step in DC-link voltage demand from 250V to 270V at  $t=2s$  was applied under RMS supply voltages  $V_a=80V$ ,  $V_b=90V$ ,  $V_c=100V$ . The load resistor was 200Ω. The result is shown in Fig.6 (a).

A step in the load ( $R_{load}$  changed from 200Ω to 92Ω) at  $t=0.85s$  was applied under RMS supply voltages  $V_a=65V$ ,  $V_b=70V$ ,  $V_c=60V$  and DC-link voltage = 185V. The experiment results are compared against the simulation results in Fig.6(b). These experiments give validation to the DP CRU model under unbalanced supply conditions.

### C. Line fault scenario

In this experiment the model was verified with a phase to ground fault on phase C. Phases A and B voltages are 80Vrms. The transient responses to a step increase in DC voltage demand from 200V to 270V at  $t = 2\text{s}$  compared in Fig.6 (c) and (d). These results show that the model accurately reproduces the dynamics of DC voltage, as well as the behaviour of CRU input currents under the phase loss.

The experimental results above confirmed that the DP CRU model is well suitable as a functional level modelling library element for normal, unbalanced and EPS line fault regimes. Figure 6 also shows that the DP CRU model accuracy is within 5% of the actual experiment as specified by the MEA functional level model requirement.

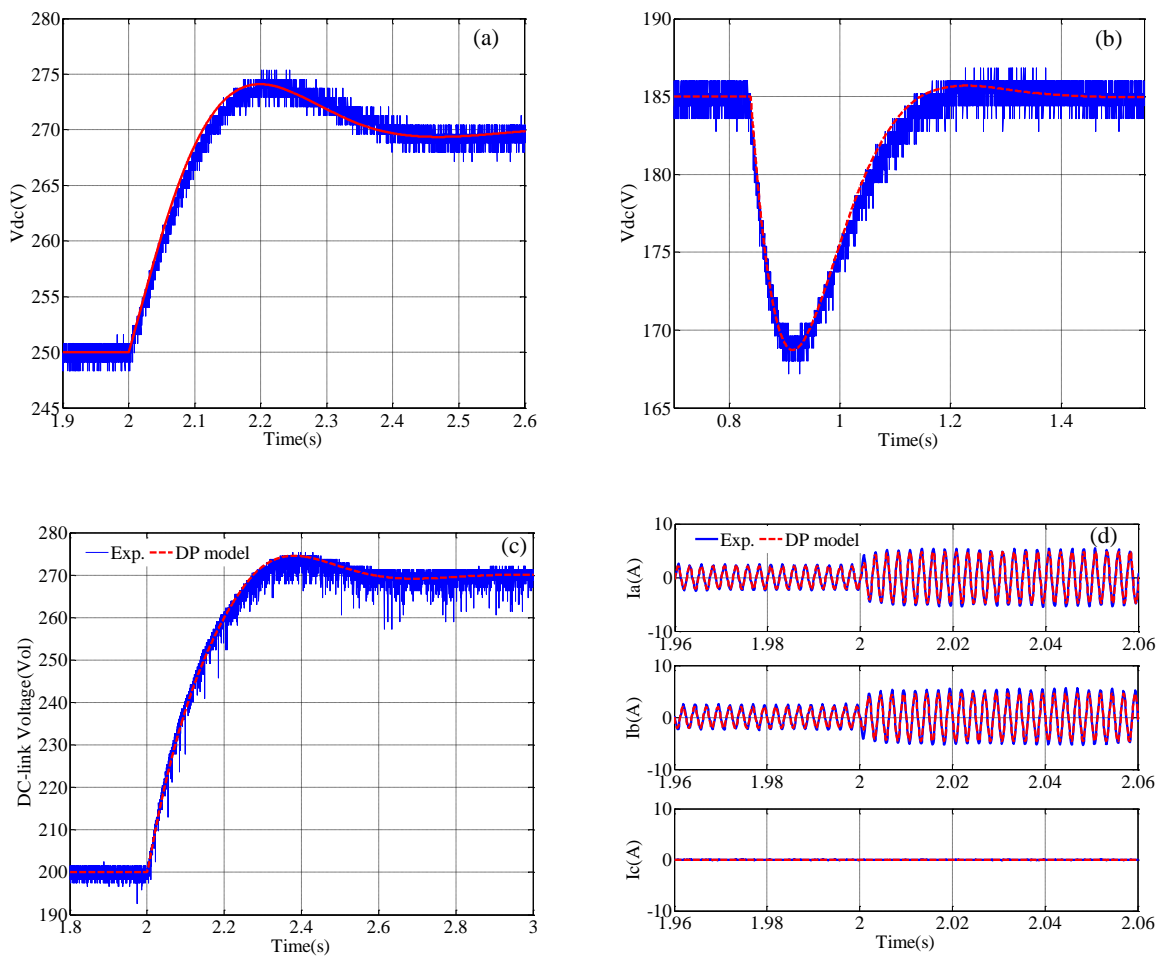


Fig. 6. Comparison between simulation and experimental results under unbalanced conditions (a)  $v_{dc}$  in response to a step in voltage demand; (b)  $v_{dc}$  with a load impact; (c)  $v_{dc}$  and (d) phase currents  $i_{abc}$  in response to a step in voltage demand under line fault conditions

## V. COMPARISON OF SIMULATION TIMES

In this section the computational effectiveness of the proposed CRU model is assessed. For this purpose, we applied different modelling techniques to an example EPS shown in Fig.7 (EPS parameters are given in Appendix II). The CPU time taken for the EPS simulation under balanced and unbalanced conditions has been monitored. We assume EPS unbalance occurs due to a line-to-line fault in the middle of the cable supplying the CRU (the cable is modelled by an RLC representation).

The following EPS models have been developed for the comparative study:

- Three-phase EPS model with switching CRU model (ideal switches). This model is illustrated by Fig.7(a) and is referred to as the abc model in the text below;
- dq0 model, in which the all AC variables in the EPS are represented in terms of synchronously rotating frame orientated on the supply voltage vector. This model is given in Fig.7(b) and is based on [5]. There are no three-phase variables in this model. The individual component models, including the functional CRU model, are as reported in [31];
- DP domain model of the whole EPS with the DP CRU model of this paper, as shown in Fig.7(c). This model does not include three-phase variables. In the text below this model is referred to as the DP model;
- An EPS model using a functional dq0 CRU model but with three-phase interfacing [31] as shown in Fig 7(d). The AC system is seen by the user as three-phase and the dq0 formulation is not visible. This model is referred to as the dq0/int model in this section;
- An EPS model using the DP CRU model of Fig.3 but with the three-phase interfacing unit of Fig.4. The AC system is seen by the user as three-phase and the DP formulation is not visible. This model is shown in Fig 7(e) and is termed the DP/int model.

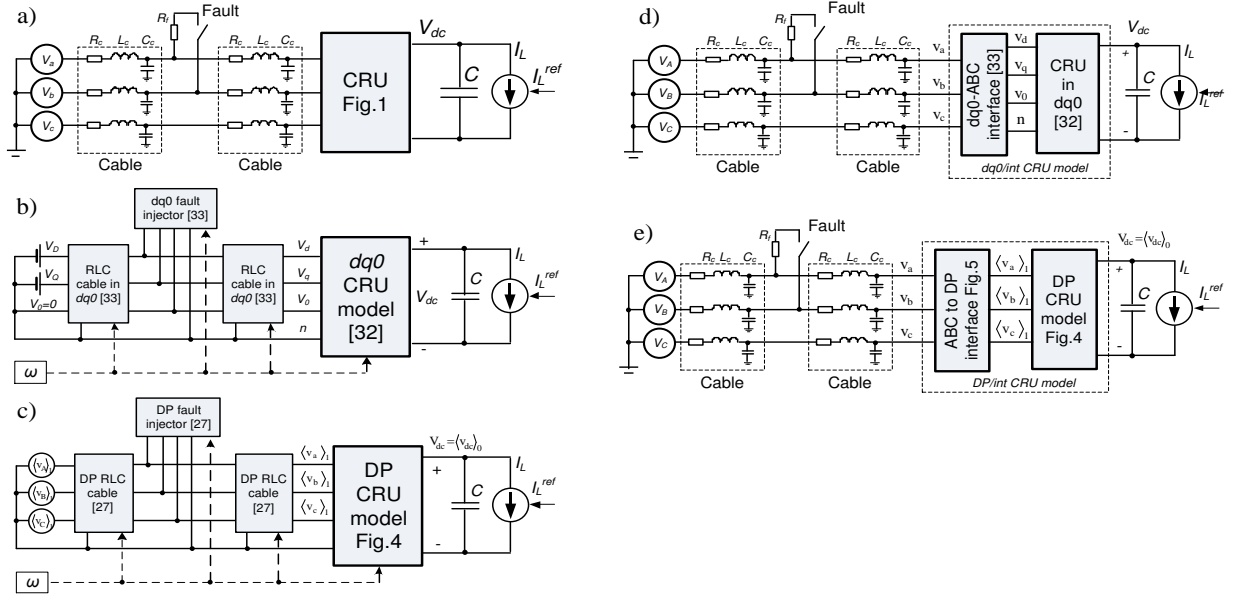


Fig.7. Example EPS modelling using different techniques

All the models were built in Modelica/Dymola v7.4 environment. The simulation scenario assumed 1s of EPS operation including a step increase of DC load current  $I_L$  from 5A to 10A occurring at  $t=0.2s$ . The simulation results are discussed below.

#### A. CPU time taken for simulation of balanced operation

The simulation results for the balanced operation scenario in Fig.8(a) confirm good accuracies of dq0 and DP models compared with the abc model. The CPU times taken by the selected models under balanced operation are given in Table III. From the Table, the dq0 model is fastest - 587 times faster than the abc model, whilst the developed DP model is 369 times faster. For this example the dq0 model is 1.6 times faster than the DP. This is consistent with expectations since the dq0 variables under balanced conditions are DC-like, and the number of system equations is less than in the DP model. The three-phase interfaced models dq0/int and DP/abc are less efficient due to additional computation required for the transformations to and from the three-phase domain. But the acceleration gained is still significant. These models are a good base for building libraries for EPS simulations.

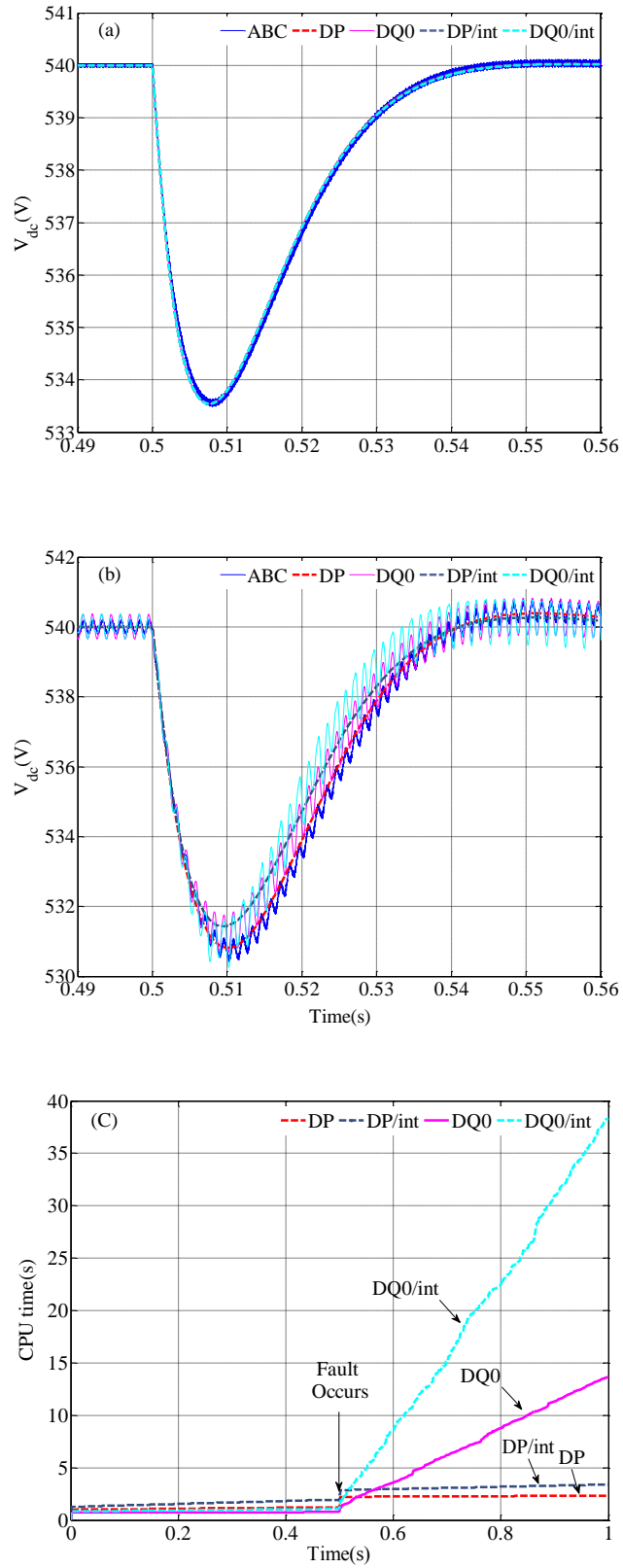


Fig. 8. Models comparison: DC-link voltage transient due to a step change in DC load under balanced and unbalanced conditions: (a) balanced conditions; (b) unbalanced conditions; (c) Computation time comparison

TABLE III. CPU TIME TAKEN FOR BALANCED SCENARIO SIMULATION

Model:	abc	dq0	DP	dq0/int	DP/int
CPU time taken:	455.5	0.774	1.232	1.092	1.935
Performance index:	<b>1</b>	<b>587</b>	<b>369</b>	<b>416</b>	<b>235</b>

### B. CPU time taken for unbalanced scenario simulation

The performance under unbalanced operation (line-to-line short between phases A and B) has been assessed. During the scenario, the same DC load current occurs as previously and the corresponding DC voltage transients are shown in Fig.8(b). As in the previous case, good accuracy of the functional models is demonstrated.

The CPU times for this scenario using different models are given Table IV. As expected, the performance of dq0 model degrades most significantly since the system variables are no longer DC-like. The dq0 model become only 35 times faster compare to the abc model. However the DP model has only slightly degraded, and is 409 times faster than the abc model, and 12 times faster than dq0 model. As one can conclude from Table IV, the DP/int model also maintains the performance during the imbalance. The simulations confirm that the DP-based models can maintain their performance in any condition. In spite of the larger number of equations in DP model compared to dq0 approach, all the system variables are still DC-like and result in larger integration time steps and faster simulations.

TABLE IV. CPU TIME TAKEN FOR UNBALANCED SCENARIO SIMULATION

Model:	abc	dq0	DP	dq0/int	DP-int
CPU time taken:	453.9	12.866	1.108	37.168	1.466
Performance index:	<b>1</b>	<b>35</b>	<b>409</b>	<b>12</b>	<b>309</b>

The performance of the above models can be illustrated by Fig.8(c) showing the cumulative CPU time during simulation. In this Figure, it was assumed that the EPS starts operation under balanced conditions, and a line-to-line fault occurs at  $t=0.5s$ . The simulations ended at  $t=1s$ . One notes that the lines corresponding to DP-based models have roughly the same gradient before and after the fault whilst the dq0-based models start to consume the CPU time at a high rate.

## VI. CONCLUSION

In this paper we have presented an active front-end rectifier model suitable for accelerated simulations of EPS's at functional level. The model maintains high computational performance under unbalanced supply voltages and line fault scenarios. This advantage was achieved by application of DPs that considers system variables as time-varying Fourier coefficients. The model has been validated experimentally. The model performance was assessed under balanced and

unbalanced conditions and for the latter, the model has proved to be much more computationally efficient compared to models using variable transformations in synchronous rotating frames. The developed CRU model has been added to the DP based modelling library for accelerated studies of future MEA EPS architectures at the functional level. This library will provide an efficient and accurate tool for system engineers to design and optimize a variety of EPS architecture candidates. Currently the library is under development and will be reported in our future publications.

#### APPENDIX I. TAYLOR SERIES COEFFICIENTS IN (21) AND (22)

$$k_{10} = f_1(V_{d0}, V_{q0}); k_{11} = \frac{\partial f_1(V_{d0}, V_{q0})}{\partial v_d}; k_{12} = \frac{\partial f_1(V_{d0}, V_{q0})}{\partial v_q}; k_{13} = \frac{\partial^2 f_1(V_{d0}, V_{q0})}{\partial v_d^2}; k_{14} = \frac{\partial^2 f_1(V_{d0}, V_{q0})}{\partial v_q^2}; k_{15} = \frac{\partial^2 f_1(V_{d0}, V_{q0})}{\partial v_d \partial v_q};$$

$$k_{20} = f_2(V_{d0}, V_{q0}); k_{21} = \frac{\partial f_2(V_{d0}, V_{q0})}{\partial v_d}; k_{22} = \frac{\partial f_2(V_{d0}, V_{q0})}{\partial v_q}; k_{23} = \frac{\partial^2 f_2(V_{d0}, V_{q0})}{\partial v_d^2}; k_{24} = \frac{\partial^2 f_2(V_{d0}, V_{q0})}{\partial v_q^2}; k_{25} = \frac{\partial^2 f_2(V_{d0}, V_{q0})}{\partial v_d \partial v_q}.$$

#### APPENDIX II. CRU MODEL PARAMETERS USED FOR SIMULATIONS

Supply:  $V_A=V_B=V_C=115V_{ph-rms}$  @400Hz. Cable (half section):  $R_c = 0.01\Omega$ ;  $L_c = 2\mu H$ ,  $C_c = 0.2nF$ . CRU: switching frequency - 10kHz;  $C = 2400mF$ . Current controllers:  $k_{pc}=23$ ,  $k_{ic}=7500$ . DC voltage controller:  $k_{pv}=0.03$ ,  $k_{iv}=0.6$ ; DC-link voltage reference – 540V.

#### ACKNOWLEDGEMENT

The author would like to thank Dr. Elisabetta Lavopa for the help in the experimental test.

#### REFERENCES

- [1] J. A. Weimer, "Electrical power technology for the more electric aircraft," in Digital Avionics Systems Conference, 1993. 12th DASC., AIAA/IEEE, 1993, pp. 445-450.
- [2] I. Moir and A. Seabridge, Aircraft Systems: mechanical, electrical, and avionics subsystems integration 3rd ed.: John Wiley & Sons, 2008.
- [3] N. Mohan, W. P. Robbins, T. M. Undeland, R. Nilssen, and O. Mo, "Simulation of power electronic and motion control systems-an overview," Proceedings of the IEEE, vol. 82, pp. 1287-1302, 1994.
- [4] T. Jomier. (2009). More Open Electrical Technologies Techincal Report. Available: <http://www.eurtd.com/moet/>. Accessed March, 2012.
- [5] S. V. Bozhko, T. Wu, C. I. Hill, and G. M. Asher, "Accelerated simulation of complex aircraft electrical power system under normal and faulty operational scenarios," in IECON 2010 - 36th Annual Conference on IEEE Industrial Electronics Society, 2010, pp. 333-338.
- [6] M. M. Jalla, A. Emadi, G. A. Williamson, and B. Fahimi, "Real time state estimation of multi-converter more electric ship power systems using the generalized state space averaging method," in Industrial Electronics Society, 2004. IECON 2004. 30th Annual Conference of IEEE, 2004, pp. 1514-1519 Vol. 2.

- [7] A. Griffio and W. Jiabin, "State-space average modelling of synchronous generator fed 18-pulse diode rectifier," in *Power Electronics and Applications*, 2009. EPE '09. 13th European Conference on, 2009, pp. 1-10.
- [8] D. Maksimovic, A. M. Stankovic, V.J.Thottuvelil, and G.C. Verghese, "Modelling and simulation of power electronic converters", *Proceedings of IEEE*, Vol. 89, Issue 6, 2001, pp. 898-912.
- [9] S. R. Sanders, J. M. Noworolski, X. Z. Liu, and G. C. Verghese, "Generalized averaging method for power conversion circuits," *Power Electronics, IEEE Transactions on*, vol. 6, pp. 251-259, 1991.
- [10] V. Venkatasubramanian, H. Schattler, and J. Zaborszky, "Fast time-varying phasor analysis in the balanced three-phase large electric power system," *IEEE Transactions on Automatic Control*, vol. 40, pp. 1975-1982, 1995.
- [11] T. Demiray, G. Andersson, and L. Busarello, "Evaluation study for the simulation of power system transients using dynamic phasor models," in *Transmission and Distribution Conference and Exposition: Latin America*, 2008 IEEE/PES, 2008, pp. 1-6.
- [12] A. M. Stankovic and T. Aydin, "Analysis of asymmetrical faults in power systems using dynamic phasors," *Power Systems, IEEE Transactions on*, vol. 15, pp. 1062-1068, 2000.
- [13] G. A. Turhan Demiray, "Simulation of Power system Dynamics using Dynamic Phasor Models," 10<sup>th</sup> Symposium of specialists in electric operational and expansion planning, Florianopolis, 2006.
- [14] B. C. L. Aleksandar, M Stankovic, Timur Aydin, "Applications of Generalized Averaging to Synchronous and Induction Machine," 28th North American Power Symposium, 1996.
- [15] Stanković, A. M., S. R. Sanders, et al., "Dynamic phasors in modelling and analysis of unbalanced polyphase AC machines," *Energy Conversion, IEEE Transactions on*, vol.17, no. 1, pp. 107-113, 2002.
- [16] T. Demiray, F. Milano, and G. Andersson, "Dynamic Phasor Modelling of the Doubly-fed Induction Generator under Unbalanced Conditions," in *Power Tech*, 2007 IEEE Lausanne, 2007, pp. 1049-1054.
- [17] A. M. Stankovic, P. Mattavelli, V. Caliskan, and G. C. Verghese, "Modelling and analysis of FACTS devices with dynamic phasors," in *Power Engineering Society Winter Meeting*, 2000. IEEE, 2000, pp. 1440-1446 vol.2.
- [18] Stefanov, P.C., Stankovic, A.M., "Dynamic Phasors in Modelling of UPFC Under Unbalanced Conditions". *Power System Technology*, 2000. *Proceedings. PowerCon 2000. International Conference on*. Vol.1., pp. 547-552.
- [19] P. Mattavelli and A. M. Stankovic, "Dynamical phasors in modelling and control of active filters," in *Circuits and Systems*, 1999. ISCAS '99. *Proceedings of the 1999 IEEE International Symposium on*, 1999, pp. 278-282 vol.5.
- [20] M. A. Hannan, A. Mohamed, and A. Hussain, "Modelling and power quality analysis of STATCOM using phasor dynamics," in *Sustainable Energy Technologies*, 2008. ICSET 2008. *IEEE International Conference on*, 2008, pp. 1013-1018.
- [21] Q. Qingru, Y. Chang, W. Chan Ka, and N. Yixin, "Modelling and simulation of a STATCOM system based on 3-level NPC inverter using dynamic phasors," in *Power Engineering Society General Meeting*, 2004. IEEE, 2004, pp. 1559-1564 Vol.2.
- [22] H. Zhu, Z. Cai, H. Liu, Q. Qi, and Y. Ni, "Hybrid-model transient stability simulation using dynamic phasors based HVDC system model," *Electric Power Systems Research*, vol. 76, pp. 582-591, 2006.
- [23] Q. Qingru, C. Shousun, V. Ni, and F. F. Wu, "Application of the dynamic phasors in modelling and simulation of HVDC," in *Advances in Power System Control, Operation and Management*, 2003. ASDCOM 2003. *Sixth International Conference on (Conf. Publ. No. 497)*, 2003, pp. 185-190.
- [24] Y. Wei, W. Jinyu, C. Shijie, and H. Haibo, "Modelling and simulation of VSC-HVDC with dynamic phasors," in *Electric Utility Deregulation and Restructuring and Power Technologies*, 2008. DRPT 2008. *Third International Conference on*, 2008, pp. 1416-1421
- [25] Venkataramanan, G., Wang, B., "Dynamic Modelling and Control of Three Phase Pulse Width Modulated Power Converters Using Phasors. *Power Electronic Specialists Conference PESC'04, Aachen, Germany*, pp.2822-2828, 2004.
- [26] Tao, Y., S. Bozhko, et al. Assessment of dynamic phasors modelling technique for accelerated electric power system simulations. *Power Electronics and Applications (EPE 2011)*, *Proceedings of the 2011-14th European Conference on*, 2011, pp. 1-9.
- [27] T. Wu, S. V. Bozhko, G. M. Asher, and D. W. Thomas, "Fast functional modelling of the aircraft power system including line fault scenarios," in *Power Electronics, Machines and Drives (PEMD 2010)*, *5th IET International Conference on*, pp. 1-7.
- [28] Wu, R., S. B. Dewan, et al. (1990). "A PWM AC-to-DC converter with fixed switching frequency." *Industry Applications, IEEE Transactions on*, **26**(5): 880-885.
- [29] S. Fukuda, Y. Iwaji, and T. Aoyama, "Modelling and control of sinusoidal PWM rectifiers," in *Power Electronics and Applications*, 1993., *Fifth European Conference on*, 1993, pp. 115-120 vol.4.
- [30] R. Pena, J. C. Clare, and G. M. Asher, "A doubly fed induction generator using back-to-back PWM converters supplying an isolated load from a variable speed wind turbine," *Electric Power Applications, IEE Proceedings -*, vol. 143, pp. 380-387, 1996.

- [31] T. Wu, S. Bozhko, G. Asher, P. Wheeler, and D. W. Thomas, "Fast Reduced Functional Models of Electromechanical Actuators for More-Electric Aircraft Power System Study," SAE International, 2008. Technical Paper 2008-01-2859.
- [32] C. Se-Kyo, "A phase tracking system for three phase utility interface inverters," Power Electronics, IEEE Transactions on, vol. 15, pp. 431-438, 2000.